Photocatalysis | **Hot Paper**

Protonated Imine-Linked Covalent Organic Frameworks for Photocatalytic Hydrogen Evolution

Jin Yang, Amitava Acharjya, Meng-Yang Ye, Jabor Rabeah, Shuang Li, Zdravko Kochovski, Sol Youk, Jérôme Roeser, Julia Grüneberg, Christopher Penschke, Michael Schwarze, Tianyi Wang, Yan Lu, Roel van de Krol, Martin Oschatz, Reinhard Schomäcker, Peter Saalfrank, and Arne Thomas*

Abstract: Covalent organic frameworks (COFs) have emerged as an important class of organic semiconductors and photocatalysts for the hydrogen evolution reaction (HER) from water. To optimize their photocatalytic activity, typically the organic moieties constituting the frameworks are considered and the most suitable combinations of them are searched for. However, the effect of the covalent linkage between these moieties on the photocatalytic performance has rarely been studied. Herein, we demonstrate that donor-acceptor (D-A) type imine-linked COFs can produce hydrogen with a rate as high as 20.7 mmol $g^{-1} h^{-1}$ under visible light irradiation, upon protonation of their imine linkages. A significant red-shift in light absorbance, largely improved charge separation efficiency, and an increase in hydrophilicity triggered by protonation of the Schiff-base moieties in the imine-linked COFs, are responsible for the improved photocatalytic performance.

Introduction

Covalent organic frameworks (COFs) are crystalline organic materials build up entirely from organic building blocks connected by covalent bonds. COFs have extended the world of organic chemistry, from molecules and polymers to 2D layered and 3D framework structures.[1] COFs possess long-range ordered micro- or small mesopores, yielding impressively high surface areas. Furthermore, owing to their

organic nature, the backbone of COFs can be equipped with a range of diverse chemical functionalities.[2] Consequently, COFs are interesting materials for applications such as gas separation and storage, electrochemical devices, and especially for catalysis.[3] Many COFs possess a pi-conjugated backbone and thus exhibit semiconducting properties. This makes them interesting materials for photocatalysis,[4] for example, for photocatalytic water splitting.[5] Polymeric carbon nitride has been the first reported metal-free photocatalyst for the hydrogen evolution from water and sparked immediate interest in this area.[5f,g] While polymeric carbon nitrides can be easily produced and are very stable materials, the high temperature synthesis (500–600 °C) however aggravate the introduction of defined chemical functions or porosities into their backbones.

As Schiff base reactions are easily achieved utilizing the vast number of amine and aldehyde functionalized monomers, imine COFs are widely studied currently.[6] Several conjugated imine COFs have been recently proven to be active photocatalysts for the hydrogen evolution reaction (HER) from water[5a,b,7] Notably, PyTA-BC-COF with pyrene and carbazole building blocks, exhibited high HER rates with ascorbic acid (AC) as the sacrificial electron donors (SEDs), while it showed negligible activity when using triethanolamine (TEOA) as the SED.[7b] By changing the halogen substitution in the benzothiadiazole monomer, it was found

---

[*] J. Yang, A. Acharjya, M.-Y. Ye, Dr. S. Li, Dr. J. Roeser, J. Grüneberg, Prof. Dr. A. Thomas
Department of Chemistry/ Functional Materials
Technische Universität Berlin
Hardenbergstraße 40, 10623 Berlin (Germany)
E-mail: arne.thomas@tu-berlin.de

Dr. J. Rabeah
Leibniz-Institut für Katalyse e.V. an der Universität Rostock
Albert-Einstein-Str. 29a, 18059 Rostock (Germany)

Dr. Z. Kochovski, Prof. Dr. Y. Lu
Institute of Electrochemical Energy Storage
Helmholtz-Zentrum Berlin für Materialien und Energie
Hahn-Meitner-Platz 1, 14109 Berlin (Germany)

S. Youk, Prof. Dr. M. Oschatz
Department of Colloid Chemistry
Max-Planck Institute of Colloids and Interfaces
Am Mühlenberg 1, 14476 Potsdam (Germany)

Dr. M. Schwarze, Prof. Dr. R. Schomäcker
Department of Chemistry, Technische Universität Berlin
Straße des 17. Juni 124, 10623 Berlin (Germany)

Dr. T. Wang, Prof. Dr. R. van de Krol
Institute for Solar Fuels
Helmholtz-Zentrum Berlin für Materialien und Energie
Hahn-Meitner-Platz 1, 14109 Berlin (Germany)

Dr. C. Penschke, Prof. Dr. P. Saalfrank
Theoretical Chemistry, Institute of Chemistry, University of Potsdam
Karl-Liebknecht-Str. 24–25, 14476 Potsdam (Germany)

that chlorinated imine COFs showed superior photocatalytic HER performance in the presence of AC.[8] Constructed from the electron-rich pyrene (Py) and electron-deficient thiazolo-[5,4- d]thiazole (Tz), PyTz-COF demonstrated a satisfying photocatalytic hydrogen evolution rate. The SED used in this work was again AC.[9] A critical analysis of these cases indicates, besides that the different building blocks naturally resulted in variations of the material properties, a rather common phenomenon, the protonation of the imine linkages is overlooked. However, it can be considered that protonation might critically influence the photocatalytic HER performance. As AC is an acidic SED for photocatalytic HER reaction, imine COFs are expected to be protonated under this reaction condition. Indeed, the protonated form of COFs was reported to exhibit distinct optical and charge carrier properties.[10] As example, when protonated by different acids, perylene-based COFs showed a remarkable red-shift in light absorption, extending even to the near-infrared spectral region.[10a] Theoretical studies of the protonation effect on imine-based discrete molecules showed that their conformation becomes more planar, leading to a higher degree of conjugation.[11] These observations are particularly important for the photocatalytic application of COFs, because such an extended conjugation would yield lower band gaps, an extended light absorption, and an enhanced charge carrier mobility and separation efficiency.[12]

In this study, the protonation effect on the photocatalytic performance of imine-COFs-based photocatalysts was investigated. Three 2D imine-linked COFs were reticulated from 2,4,6-Tris(4-aminophenyl)triazine (Tta), Tris(4-formylphenyl)amine (Tfa), 1,3,5-Tris(4-formylphenyl)benzene (Tpa-CHO) and 1,3,5-Tris(4-aminophenyl)benzene (Tpa-NH$_2$) as building blocks. The three COFs (TtaTfa, TpaTfa, TtaTpa) were previously reported and proved to be synthetically accessible under mild solvothermal conditions.[3b,13] The triazine core of Tta is electron deficient, thus acting as an acceptor building block.[14] In contrast, the triphenylamine motif in Tfa is a well-known electron donor.[15] Finally, the triphenylbenzene motif in the Tpa monomers can serve as both donor and acceptor depending on the other building blocks. Donor–acceptor (D-A) motifs within COFs have been demonstrated to be effective to tune their electronic properties.[4a,16] Thus, the as-

synthesized imine COFs are expected to possess photocatalytic activity to a different extent. To compare the property change with the pristine COFs, the protonated counterparts of these imine COFs were then synthesized and characterized. As will be described below, these imine COFs showed remarkably high activity as photocatalysts for HER but just when using AC as SED.

Results and Discussion

Applying the described building blocks, three imine-linked COFs with related structures but variable D-A moieties within the backbone were synthesized (Figure 1). The high crystallinity and porous structure of the COFs were confirmed by a combination of powder X-ray diffraction (PXRD), gas sorption, and transmission electron microscopy (TEM) analyses (Figure 2; Supporting Information, Figures S1–S4). As an example, the experimental PXRD pattern of TtaTfa showed intense and sharp diffraction peaks, which matched well with the simulated AA stacking patterns (Figure 2a). From the nitrogen (N$_2$, at 77 K) and argon (Ar, at 87 K) sorption measurements, TtaTfa showed high porosity and a narrow pore size distribution (Figure 2b, c, Figure S2, S3). The Brunauer–Emmett–Teller (BET) surface area of TtaTfa was calculated to be 1258 m^{2}g^{-1} from Ar sorption (calculated theoretical BET surface area 2245 m^{2}g^{-1}). The
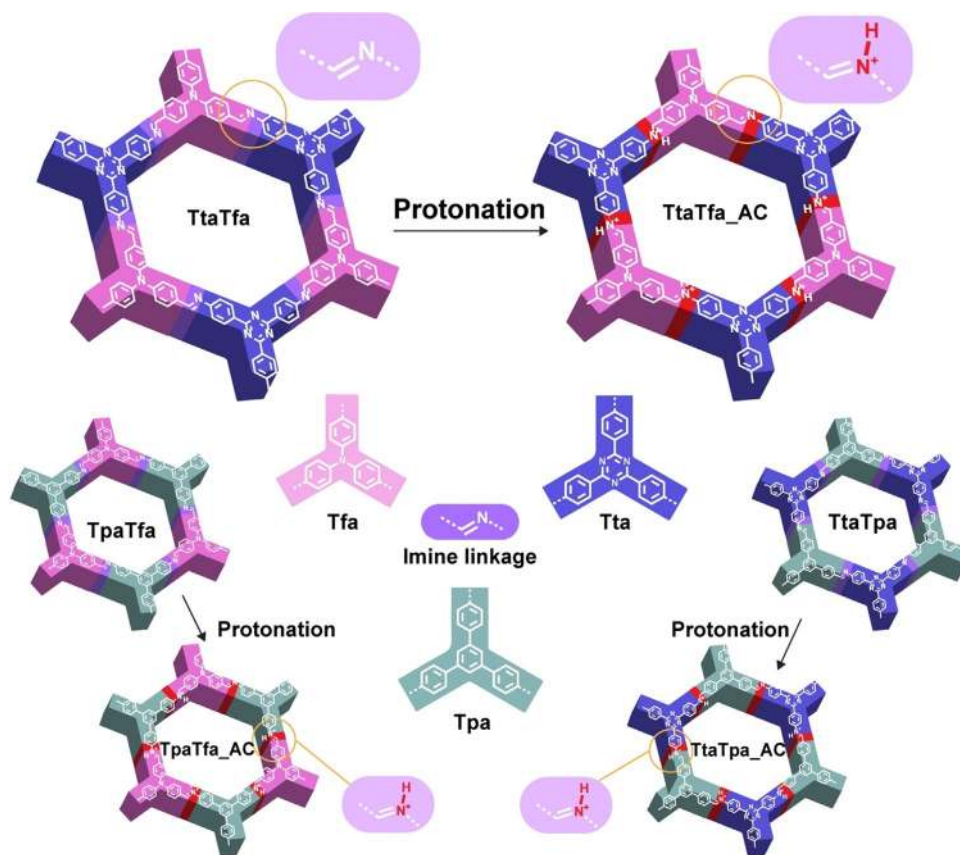
Figure 1. Synthesis of the COFs studied in this work. Scheme of synthesis of TtaTfa, TtaTfa AC, TpaTfa, TpaTfa AC, TtaTpa, and TtaTpa AC. AC = ascorbic acid modification.
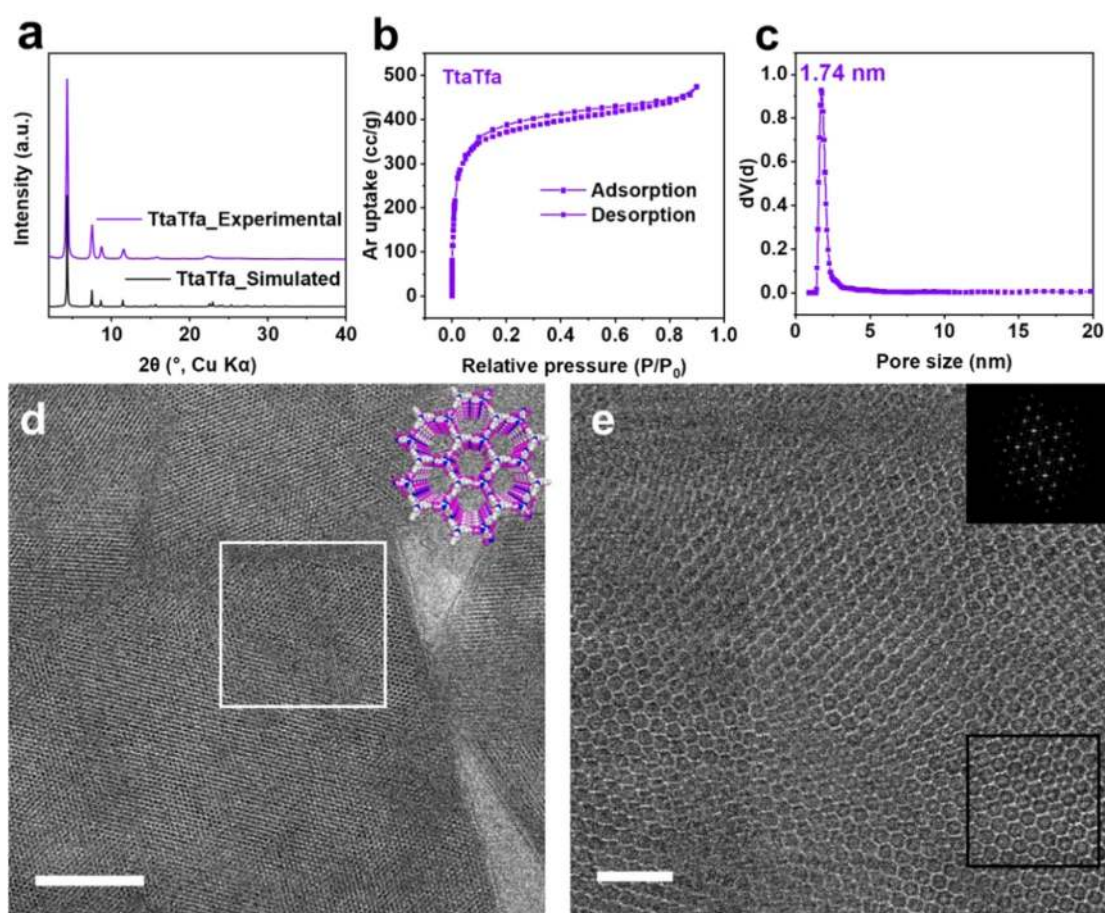
Figure 2. Characterization of TtaTfa. a) Experimental PXRD patterns of TtaTfa compared with the simulated eclipsed-stacking (AA) PXRD pattern. b) Argon isotherm of TtaTfa. c) Calculated pore size distribution plot of TtaTfa from Argon adsorption data at 87 K after QSDFT model fitting of adsorption branch data. d) Low-dose TEM image of TtaTfa under cryogenic conditions (scale bar: 50 nm). e) Low-dose HRTEM image under cryogenic conditions of the region indicated by white square in d (scale bar: 10 nm). The inset in e shows a Fast Fourier Transform (FFT) of the region indicated by the black square.

experimental pore size distribution was derived from Ar adsorption data and determined to be centered at 1.74 nm for TtaTfa, which is close to the theoretical value (1.91 nm). Some amount of offset stacking besides the ideal AA stacking might be responsible for the deviation from the theoretical values. The periodic framework structural features of TtaTfa were visualized by low-dose, high-resolution transmission electron microscopy (HRTEM) (Figure 2d and e). As shown in Figure 2d and 2e, the large domains of 2D hexagonal honeycomb-type pore structure can be clearly observed along the [001] direction. The direct observation of the chemical structures matches well with the PXRD and gas sorption results. Fourier transform infrared spectroscopy (FTIR) results confirmed the completion of the reaction and the formation of imine bonds within the COFs from the Schiff base reaction (Figure S5). The morphology of the COFs was observed by scanning electron microscopy (SEM) measurements, showing irregular, sheet-like structures (Figure S6). The TpaTfa and TtaTpa COFs were analyzed correspondingly and showed as well high structural order and porosity with surface areas of 972 and 747 $m^2 g^{-1}$ from Ar sorption, respectively (Figures S1-S6). After confirming the structural homogeneity of the pristine imine COFs, the AC modified

COFs were isolated after a 5 minutes treatment in 0.1 M AC aqueous solution followed by filtration and an overnight ultra-high vacuum drying step at room temperature. AC was used as acid, because it was also used during the photocatalytic tests as the sacrificial agent. An obvious effect of AC treatment for all three COFs was observed in form of a remarkable color change (inset of Figure 3a, Figure S7), which occurred within seconds (Supplementary Video 1). The color of TpaTfa and TtaTfa both changed from bright yellow to deep-red, and TtaTpa turned from pale yellow to orange. Ultraviolet-visible diffuse reflectance spectroscopy (UV/Vis DRS) measurements confirmed the enhanced light absorption of the three imine COFs after AC treatment (Figure 3a, Figure S7). The absorption onsets of pristine TpaTfa, TtaTfa and TtaTpa are located at 493 nm, 507 nm and 476 nm, respectively. After protonation these absorption onsets redshift to 687 nm, 688 nm and 604 nm, respectively. This redshift cannot be attributed to the absorbance of the added AC, as it is a colorless compound, which does not absorb light in visible-light range (Figure S8). The calculated band gaps from Tauc plots are 2.60, 2.52, and 2.73 eV for pristine TpaTfa, TtaTfa and TtaTpa, respectively, which narrow down significantly to 1.89, 1.90, and 2.22 eV after treatment with AC
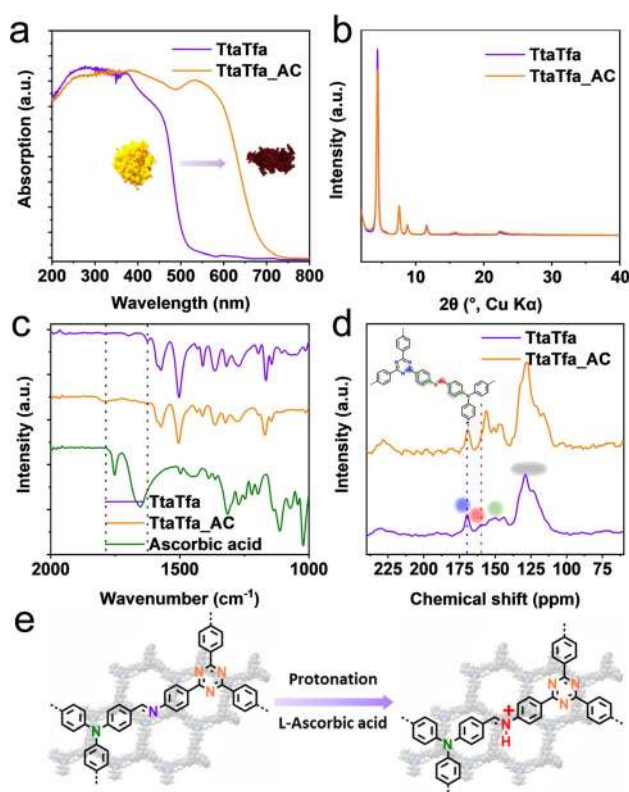
Figure 3. a) UV/Vis DRS spectra of TtaTfa before and after AC treatment (Inset: corresponding photographs of TtaTfa and TtaTfa_AC). Comparison of the PXRD patterns b) FTIR spectra c) and ^{13}C solid-state MAS NMR spectra d) of TtaTfa and TtaTfa_AC. e) The protonation of TtaTfa with L-Ascorbic acid.

(Figure S7). After AC modification the relative intensity ratio of the reflections in the PXRD patterns changed slightly, due to the presence of ascorbate anions within the pores (Figure 3b, S9). All the AC modified COFs also showed a decreased surface area due to the presence of those guest molecules (Figure S10). However, AC modification did not change the morphology (Figure S11). The light absorption of TtaTfa at different pH values illustrates its gradual protonation (Figure S7d).[10a] Besides AC, other acids such as hydrochloric acid can also trigger the color change of the synthesized imine COFs (Figure S12).

Fast and reversible color change in COFs upon protonation/deprotonation has been observed before and it was demonstrated that such systems could be applied as acidic/basic chemosensor.[10] Thus, the protonation of the imine groups within the COFs is the most obvious explanation for the changes. However, both triazine and amine moieties are basic sites, which might be also protonated. Nevertheless, estimated pKa values of the conjugated acid of 2,4,6-triphenyl-1,3,5-triazine (pKa = 1.8), triphenylamine (pKa < 2), and phenyl-substituted imines (pKa = 5–7) showed that the imine groups are the strongest basic sites.[17] As the pK$_a$ value of AC is 4.2 in water at 25 °C, it can be assumed that just the imine sites can be protonated by AC. In the FTIR spectra, the stretching frequency around 1623 cm^{-1}, which is assigned as the stretching mode of imine bonds, disappeared or

attenuated after modification of the COFs with AC. Moreover, a broad new peak appeared at around 1791 cm^{-1}, which cannot be assigned to free AC but to the newly formed C=NH${}^+$ bond (Figure 3c, S13).[10a] ^{13}C cross polarization magic angle spinning (CP-MAS) NMR spectroscopy measurement (Figure 3d) showed that compared to pristine TtaTfa, the signal assigned to the imine carbon atom of TtaTfa AC experienced an obvious shift to higher fields, while the signals assigned to the triazine carbon and the carbon close to the amine nitrogen remained almost unchanged.[10b] These results indicate that protonation occurs exclusively at the imine sites within the COFs (Figure 3e).

We performed density functional theory (DFT) calculations on cluster models mimicking one pore of TtaTfa to analyze the electronic structure (see the Supporting Information for details). The observed red-shift upon protonation is consistent with quantum chemical calculations. Using CAM-B3LYP, protonation of a single imine group reduces the HOMO–LUMO gap of TtaTfa from 5.52 eV (225 nm) to 2.13 eV (583 nm). Protonation of all six imine groups within the pore leads also to a red-shift, albeit to a lesser extent (compare Table S1). Both HOMO and LUMO are shifted to lower energies upon protonation. We also calculated transition energies and probabilities using time-dependent DFT, which can be more directly compared to UV-vis spectra. The lowest excitation energy with non-vanishing oscillator strength of TtaTfa is 3.72 eV (334 nm), which is reduced to 2.40 eV (518 nm) upon single protonation and to 2.64 eV (469 nm) upon full protonation. Analysis of the corresponding natural transition orbitals (NTOs, see SI, Figure S14, 15) shows that donor and acceptor orbitals typically involve the same set of atoms, with some small amount of charge transfer in case of the (singly) protonated species.

After elucidating the changes in chemical structure and electronic properties of imine COFs before and after protonation with AC, it can be assumed that such a protonation should have a significant effect on their photocatalytic activity. To investigate this effect, besides AC (acidic), TEOA (alkaline) was also applied as SED.[23] The distinct color change of the imine COFs in AC aqueous dispersion is identical to the one in the solid-state, while their color remained almost unchanged in TEOA aqueous solutions (Figure 4d, S16). All imine COFs synthesized in this study showed remarkable photocatalytic HER activity when AC was used as SED and Pt as co-catalyst (Figure 4a, b). TtaTfa with the strongest D-A pair in the backbone showed the highest HER rate of 20.7 ± 2.7 mmol g^{-1} h^{-1} (Supplementary Video 2). Likewise, TpaTfa with a weak acceptor and strong donor or TtaTpa with strong acceptor and weak donor could evolve H$_2$ with a decent rate of 14.9 ± 1.1 mmol g^{-1} h^{-1} and 10.8 ± 0.8 mmol g^{-1} h^{-1}, respectively. These values compare well to the activities reported so far for pure COF materials (Table S2). The activity of TtaTfa is also comparable to the most active COF-related photocatalyst, that is, a MOF/COF composite NH$_2$-UiO-66/TpPa-1-COF in photocatalytic HER.[7c] However, this picture changed completely when conducting photocatalysis with TEOA as a sacrificial agent, as in this case, only TtaTpa exhibits some activity (Figure 4c). It should be noted that differences in the oxidation potential of
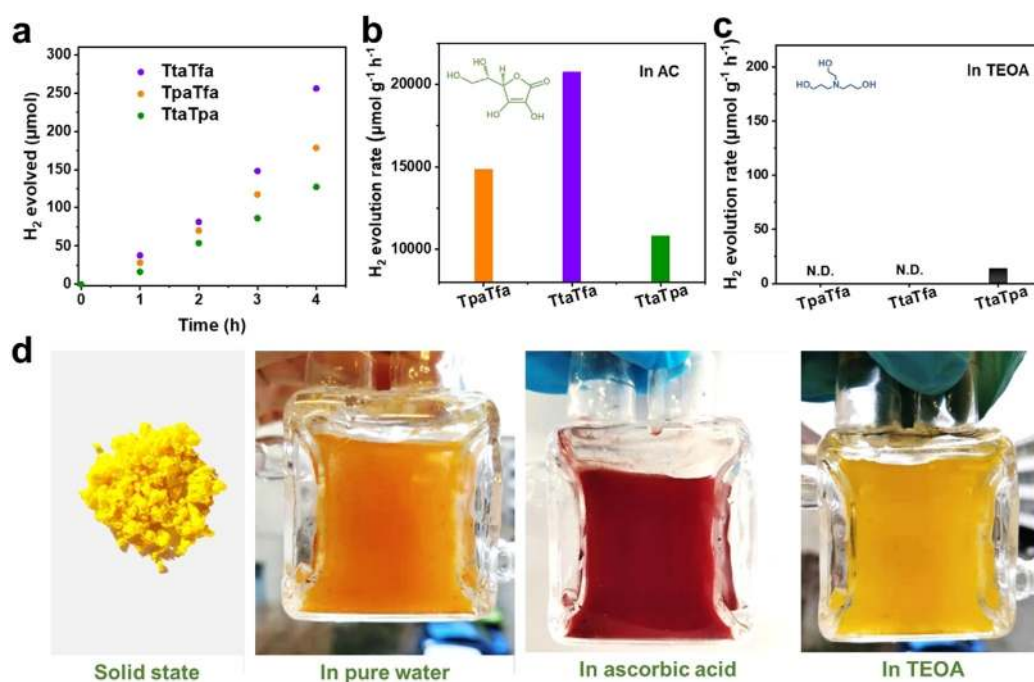
Figure 4. a) Time course of photocatalytic H$_2$ evolution for TtaTfa, TpaTfa, and TtaTpa using AC as SED (3 mg catalyst, 16 mL 0.1 M AC aqueous solution, 3 μL H$_2$PtCl$_6$ (8 wt%), λ > 420 nm, 20°C). Comparison of photocatalytic HER rates of the above COFs using AC as SED b) and using TEOA as SED (5 mg catalyst, 16 mL water, 2 mL TEOA, 5 μL H$_2$PtCl$_6$ (8 wt%), λ > 420 nm, 20°C) c). d) Color of TtaTfa powder and dispersion at different reaction conditions.

the two sacrificial electron donors could account for a partial lower performance of the COFs when TEOA is applied, but probably not for a total loss in activity. To confirm the source of hydrogen in the evolved H$_2$, hydrogen isotope labeling experiments were performed in pure D$_2$O (Figure S17). The gained mass spectra clearly confirmed that the generated gas was mostly D$_2$, which cannot be formed from any other sources than water. The small amount of H in H$_2$ and HD presumably originate from the proton in AC or H$_2$PtCl$_6$ aqueous solution. Furthermore, a control experiment in the absence of any SED was conducted (Figure S18a). It should be mentioned that when adding H$_2$PtCl$_6$ to the solution for the in situ photodeposition of Pt, the reaction solution becomes acidic as well. Thus, also in the tests without SED, protonation of the imine COFs can be assumed (Figure S16, Table S3). TtaTpa showed some activity in hydrogen evolution even without any SED; however, no O$_2$ evolution could be detected. This might be explained by the negligible amount of O$_2$ formation which can mostly remain dissolved in the reaction media since O$_2$ has a circa 25x higher solubility in water than H$_2$. In contrast, TtaTfa and TpaTfa showed no activity for HER at all, when no SED is used. Thus, the latter COFs, even though highly active for hydrogen evolution in acidic media, might not be suitable alone for overall water splitting, but would be certainly interesting for the cathodic part of a Z-scheme photocatalyst. The apparent quantum efficiency (AQE) was measured for the most active COF TtaTfa. An AQE of 1.43% at 450 nm and 0.03% at 520 nm was reached. Photocatalytic tests were also carried out at different pH values. TtaTfa is only active in acidic conditions with an optimum performance at pH 2.5, while at lower or

higher pH values a decreased activity is observed. (Figure S18). After photocatalysis, all COFs were recovered and the structural integrity was investigated by PXRD and FTIR. A small decrease of crystallinity was observed for the recovered COFs, but in contrast to other COFs used in photocatalysis, do not lose their structural order entirely (Figure S19).[8,18] Moreover, no change in the imine backbone can be spotted by FTIR analysis (Figure S20). This remarkable stability may originate from the well-crystallized framework structure,[7d,10a] furthermore protonation might also prevent the photocatalyst from being oxidized by its own holes to a certain extent, which would also deactivate the photocatalyst. A long-term photocatalytic experiment was conducted by applying TtaTfa (Figure S21a). The H$_2$ can continuously evolve for at least 26 hours. After this test, however, the crystalline structure has strongly attenuated (Figure S21b).

As shown, protonation of the COFs reduces their band gaps thus they absorb a larger fraction of the visible spectrum, which could explain the strong increase in activity. However, light absorption only accounts for the initial step of photocatalysis, while the subsequent charge separation and recombination steps usually limit the overall performance.[4b,19] Electron paramagnetic resonance spectroscopy (EPR) is a contactless and effective method to evaluate the charge separation efficiency of photocatalysts.[20] Here, the conduction band electrons (CB e$^-$) were monitored by EPR before and after visible light irradiation. Generally, all samples showed an EPR signal at $g = 2.007$, which is attributed to photoexcited electrons in the conduction band indicating the photochemical generation of electron–hole pairs in the COF

catalysts. TtaTfa_AC exhibited a much higher signal intensity than the pristine COF TtaTfa, which suggests a largely improved charge separation efficiency of the protonated COF, TtaTfa_AC (Figure 5a, b). The remarkably enhanced EPR signal is also observed for TpaTfa, TtaTpa, and their protonated counterparts, TpaTfa_AC, TtaTpa_AC (Figure 5c, S22). Moreover, the charge recombination process is less pronounced for the protonated counterpart of the COFs, especially over the most active TtaTfa_AC (Figure S23). The origin of the better charge separation can be attributed to the stabilization and delocalization of the unpaired electron over the frameworks. As more CB e$^-$ are generated, which can take part in the proton reduction, higher amount of H$_2$ can be generated finally. The improvement of the charge separation efficiency is consistent with the photocatalytic performance trend. Another critical factor that affects the water splitting performance, is the polarity of the photocatalyst, as hydrophilic pore surfaces are better accessible to water and also yield a better dispersibility of the catalyst powder in water.[21] Therefore, water sorption experiments were conducted (Figure 5d, S24). Hydrophilicity/hydrophobicity can be determined by the uptake at low relative pressure (usually p/p$_0$ = 0.2–0.4). At p/p$_0$ = 0.2 (298 K), the water uptake of TtaTfa_AC (1.3 mmol g^{-1}) is three times higher than TtaTfa (0.43 mmol g^{-1}). Even though the pore volume decreased due to the introduction of AC, TtaTfa_AC still showed more total water uptake with the uptake of 27.5 mmol g^{-1} than TtaTfa with the uptake of 20.2 mmol g^{-1} at p/p$_0$ = 0.9 (298 K). These results prove that the protonated counterparts of the imine COFs are more hydrophilic than the pristine materials.[22] Thus, protonation of the imine moieties in the COF backbone also promotes the water accessibility of the COFs pores which also attributes to their enhanced performance as water splitting photocatalysts.

Conclusion

Three highly crystalline imine COFs reticulated with alternating D-A moieties of different strengths were synthesized. These imine COFs show high photocatalytic HER reactivity when applying an acidic SED (ascorbic acid), while only negligible amount of H$_2$ was produced in alkaline condition (TEOA as SED). In ascorbic acid, the COF TtaTfa which combines the strongest acceptor (triazine) and strongest donor (triphenylamine) moieties exhibits the best photocatalytic HER performance of all tested COFs, reaching a remarkable HER rate of 20.7 mmol g^{-1} h^{-1}. The less active COFs TpaTfa and TtaTpa still generate H$_2$ with high rates of 14.9 mmol g^{-1} h^{-1} and 10.8 mmol g^{-1} h^{-1}, respectively. The high photocatalytic HER activity of these COFs is attributed to the protonation of the imine linkage. Detailed analysis of the chemical and electronic properties suggest that protonation has multiple beneficial effects, all enhancing the photocatalytic performance of these materials. Firstly, protonation enhances the light absorption ability, secondly promotes the charge separation efficiency, and finally increases the hydrophilicity of the COFs. This work reports the effect of linkage modification on COFs properties, and reveals the remarkable effect of protonation of imine COFs for photocatalytic HER. Furthermore, this phenomenon is also instructive for other application fields of COFs where tunability of their semiconducting properties is important.
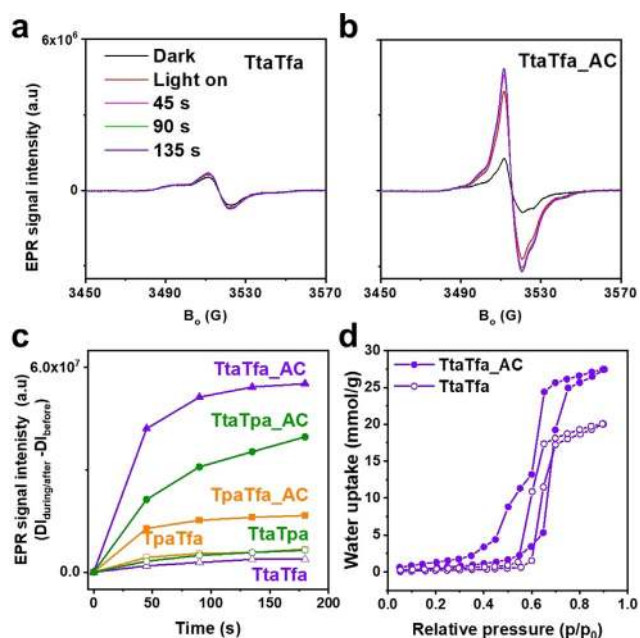
Figure 5. EPR conduction band electrons spectra of TtaTfa a) and TtaTfa_AC b) in the dark and during visible light irradiation (>420 nm, 300 W Xe lamp). c) The double integration of the conduction band electron signal of TtaTfa, TtaTfa_AC, TpaTfa, TpaTfa_AC, TtaTpa, and TtaTpa_AC after subtraction the corresponding reference spectrum in dark. d) Water sorption analysis on TtaTfa and TtaTfa_AC at 298 K.

Conflict of Interest

The authors declare no conflict of interest.

[1] a) C. S. Diercks, O. M. Yaghi, *Science* **2017**, *355*, eaal1585; b) N. Chaoui, M. Trunk, R. Dawson, J. Schmidt, A. Thomas, *Chem. Soc. Rev.* **2017**, *46*, 3302–3321.

[2] X. Chen, K. Geng, R. Liu, K. T. Tan, Y. Gong, Z. Li, S. Tao, Q. Jiang, D. Jiang, *Angew. Chem. Int. Ed.* **2020**, *59*, 5050–5091; *Angew. Chem.* **2020**, *132*, 5086–5129.

[3] a) S. Kandambeth, K. Dey, R. Banerjee, *J. Am. Chem. Soc.* **2019**, *141*, 1807–1822; b) A. F. M. El-Mahdy, C. H. Kuo, A. Alshehri, C. Young, Y. Yamauchi, J. Kim, S. W. Kuo, *J. Mater. Chem. A* **2018**, *6*, 19532–19541.

[4] a) P. Pachfule, A. Acharjya, J. Roeser, R. P. Sivasankaran, M. Y. Ye, A. Bruckner, J. Schmidt, A. Thomas, *Chem. Sci.* **2019**, *10*, 8316–8322; b) Q. Wang, K. Domen, *Chem. Rev.* **2020**, *120*, 919–985.

[5] a) P. Pachfule, A. Acharjya, J. Roeser, T. Langenhahn, M. Schwarze, R. Schomacker, A. Thomas, J. Schmidt, *J. Am. Chem. Soc.* **2018**, *140*, 1423–1427; b) X. Y. Wang, L. J. Chen, S. Y. Chong, M. A. Little, Y. Z. Wu, W. H. Zhu, R. Clowes, Y. Yan, M. A. Zwijnenburg, R. S. Sprick, A. I. Cooper, *Nat. Chem.* **2018**, *10*, 1180–1189; c) Y. Y. Wan, L. Wang, H. X. Xu, X. J. Wu, J. L. Yang, *J. Am. Chem. Soc.* **2020**, *142*, 4508–4516; d) X. Huang, Y.-B. Zhang, *Chem. Lett.* **2021**, *50*, 676–686; e) J. Corredor, M. J. Rivero, C. M. Rangel, F. Gloaguen, I. Ortiz, *J. Chem. Technol. Biotechnol.* **2019**, *94*, 3049–3063; f) X. Wang, K. Maeda, A. Thomas, K. Takanabe, G. Xin, J. M. Carlsson, K. Domen, M. Antonietti, *Nat. Mater.* **2009**, *8*, 76–80; g) L. Lin, Z. Lin, J. Zhang, X. Cai, W. Lin, Z. Yu, X. Wang, *Nat. Catal.* **2020**, *3*, 649–655.

[6] a) J. L. Segura, M. J. Mancheno, F. Zamora, *Chem. Soc. Rev.* **2016**, *45*, 5635–5671; b) S. Y. Ding, J. Gao, Q. Wang, Y. Zhang, W. G. Song, C. Y. Su, W. Wang, *J. Am. Chem. Soc.* **2011**, *133*, 19816–19822.

[7] a) B. P. Biswal, H. A. Vignolo-Gonzalez, T. Banerjee, L. Grunenberg, G. Savasci, K. Gottschling, J. Nuss, C. Ochsenfeld, B. V. Lotsc, *J. Am. Chem. Soc.* **2019**, *141*, 11082–11092; b) A. F. M. El-Mahdy, A. M. Elewa, S. W. Huang, H. H. Chou, S. W. Kuo, *Adv. Opt. Mater.* **2020**, *8*, 2000641; c) F. M. Zhang, J. L. Sheng, Z. D. Yang, X. J. Sun, H. L. Tang, M. Lu, H. Dong, F. C. Shen, J. Liu, Y. Q. Lan, *Angew. Chem. Int. Ed.* **2018**, *57*, 12106–12110; *Angew. Chem.* **2018**, *130*, 12282–12286; d) V. S. Vyas, F. Haase, L. Stegbauer, G. Savasci, F. Podjaski, C. Ochsenfeld, B. V. Lotsch, *Nat. Commun.* **2015**, *6*, 8508.

[8] W. B. Chen, L. Wang, D. Z. Mo, F. He, Z. L. Wen, X. J. Wu, H. X. Xu, L. Chen, *Angew. Chem. Int. Ed.* **2020**, *59*, 16902–16909; *Angew. Chem.* **2020**, *132*, 17050–17057.

[9] W. Li, X. Huang, T. Zeng, Y. A. Liu, W. Hu, H. Yang, Y. B. Zhang, K. Wen, *Angew. Chem. Int. Ed.* **2021**, *60*, 1869–1874.

[10] a) L. Ascherl, E. W. Evans, J. Gorman, S. Orsborne, D. Bessinger, T. Bein, R. H. Friend, F. Auras, *J. Am. Chem. Soc.* **2019**, *141*, 15693–15699; b) R. Kulkarni, Y. Noda, D. Kumar Barange, Y. S. Kochergin, P. Lyu, B. Balcarova, P. Nachtigall, M. J. Bojdys, *Nat. Commun.* **2019**, *10*, 3228.

[11] a) Y. Z. Xie, G. G. Shan, Z. Y. Zhou, Z. M. Su, *Sens. Actuators B Chem.* **2013**, *177*, 41–49; b) F. Wang, T. Qi, Z. Su, Y. Xie, *J. Mol. Model.* **2018**, *24*, 58.

[12] Y. H. Wijsboom, A. Patra, S. S. Zade, Y. Sheynin, M. Li, L. L. W. Shimon, M. Bendikov, *Angew. Chem. Int. Ed.* **2009**, *48*, 5443–5447; *Angew. Chem.* **2009**, *121*, 5551–5555.

[13] a) B. C. Patra, S. K. Das, A. Ghosh, K. A. Raj, P. Moitra, M. Addicoat, S. Mitra, A. Bhaumik, S. Bhattacharya, A. Pradhan, *J. Mater. Chem. A* **2018**, *6*, 16655–16663; b) L. P. Zhai, N. Huang, H. Xu, Q. H. Chen, D. L. Jiang, *Chem. Commun.* **2017**, *53*, 4242–4245.

[14] A. Acharjya, P. Pachfule, J. Roeser, F. J. Schmitt, A. Thomas, *Angew. Chem. Int. Ed.* **2019**, *58*, 14865–14870; *Angew. Chem.* **2019**, *131*, 15007–15012.

[15] Y. Liao, H. Wang, M. Zhu, A. Thomas, *Adv. Mater.* **2018**, *30*, 1705710.

[16] a) S. B. Jin, K. Furukawa, M. Addicoat, L. Chen, S. Takahashi, S. Irle, T. Nakamura, D. L. Jiang, *Chem. Sci.* **2013**, *4*, 4505–4511; b) M. Calik, F. Auras, L. M. Salonen, K. Bader, I. Grill, M. Handloser, D. D. Medina, M. Dogru, F. Lobermann, D. Trauner, A. Hartschuh, T. Bein, *J. Am. Chem. Soc.* **2014**, *136*, 17802–17807; c) Y. S. Kochergin, D. Schwarz, A. Acharjya, A. Ichangi, R. Kulkarni, P. Eliasova, J. Vacek, J. Schmidt, A. Thomas, M. J. Bojdys, *Angew. Chem. Int. Ed.* **2018**, *57*, 14188–14192; *Angew. Chem.* **2018**, *130*, 14384–14388.

[17] a) F. Elbe, J. Keck, A. P. Fluegge, H. E. A. Kramer, P. Fischer, P. Hayoz, D. Leppard, G. Rytz, W. Kaim, M. Ketterle, *J. Phys. Chem. A* **2000**, *104*, 8296–8306; b) J. E. Rice, *Organic Chemistry Concepts and Applications for Medicinal Chemistry*, Academic Press, an imprint of Elsevier, San Diego, CA, **2014**, p. 79.

[18] a) L. Stegbauer, K. Schwinghammer, B. V. Lotsch, *Chem. Sci.* **2014**, *5*, 2789–2793; b) L. Stegbauer, S. Zech, G. Savasci, T. Banerjee, F. Podjaski, K. Schwinghammer, C. Ochsenfeld, B. V. Lotsch, *Adv. Energy Mater.* **2018**, *8*, 1703278.

[19] a) C. H. Dai, B. Liu, *Energy Environ. Sci.* **2020**, *13*, 24–52; b) Y. O. Wang, A. Vogel, M. Sachs, R. S. Sprick, L. Wilbraham, S. J. A. Moniz, R. Godin, M. A. Zwijnenburg, J. R. Durrant, A. I. Cooper, J. W. Tang, *Nat. Energy* **2019**, *4*, 746–760.

[20] a) D. Hollmann, M. Karnahl, S. Tschierlei, K. Kailasam, M. Schneider, J. Radnik, K. Grabow, U. Bentrup, H. Junge, M. Beller, S. Lochbrunner, A. Thomas, A. Bruckner, *Chem. Mater.* **2014**, *26*, 1727–1733; b) A. Indra, A. Acharjya, P. W. Menezes, C. Merschjann, D. Hollmann, M. Schwarze, M. Aktas, A. Friedrich, S. Lochbrunner, A. Thomas, M. Driess, *Angew. Chem. Int. Ed.* **2017**, *56*, 1653–1657; *Angew. Chem.* **2017**, *129*, 1675–1679.

[21] a) S. Q. Zhang, G. Cheng, L. P. Guo, N. Wang, B. E. Tan, S. B. Jin, *Angew. Chem. Int. Ed.* **2020**, *59*, 6007–6014; *Angew. Chem.* **2020**, *132*, 6063–6070; b) W. Zhou, Z. C. Hu, F. Huang, W. Hong, X. D. Chen, *Appl. Catal. B Environ.* **2020**, *270*, 118852.

[22] N. Popp, T. Homburg, N. Stock, J. Senker, *J. Mater. Chem. A* **2015**, *3*, 18492–18504.

[23] J. Z. Cheng, L. L. Liu, G. Liao, Z. Q. Shen, Z. R. Tan, Y. Q. Xing, X. X. Li, K. Yang, L. Chen, S. Y. Liu, *J. Mater. Chem. A* **2020**, *8*, 5890–5899.